land

MDPI

*Article*

# Distribution Characteristics and Relationship Between Soil Salinity and Soil Particle Size in Ebinur Lake Wetland, Xinjiang

**Duo Wen [1,2,3,†], Jinjie Wang [1,2,3,†], Jianli Ding [1,2,3,4,*] and Zhe Zhang [1,2,3]**

[1] College of Geography and Remote sensing Science, Xinjiang University, Urumqi 830017, China; 107552201166@stu.xju.edu.cn (D.W.); wangjj@xju.edu.cn (J.W.); zhangzhe_0110@yeah.net (Z.Z.)
[2] Xinjiang Key Laboratory of Oasis Ecology, Xinjiang University, Urumqi 830017, China
[3] Key Laboratory of Smart City and Environment Modelling of Higher Education Institute, Xinjiang University, Urumqi 830017, China
[4] Xinjiang Institute of Technology, Aksu 843000, China
* Correspondence: dingjl@xju.edu.cn; Tel.: +86-135-7926-5967
† These authors contributed equally to this work.

**Abstract:** A comprehensive understanding of soil salinity characteristics and the vertical and spatial distribution of particle sizes in lakes and wetlands within arid zones, as well as elucidating their interrelationship, is crucial for effective wetland soil salinization management. In this study, the typical salinized wetland, the Ebinur Lake wetland, was selected as the research object. A total of 50 sampling points were established along the edge of Ebinur Lake, resulting in the collection of 200 soil samples from depths of 0–60 cm. The particle size distribution (PSD) of the soil samples was obtained by laser particle sizer, and the fractal dimension of the soil structure was deduced by applying fractal theory. The soluble salt content (TSS) and salt ions content were measured by laboratory physicochemical experiments. Finally, Pearson correlation and other methods were used to explore the relationship between soil salinity and soil particle size. The results showed the following: (1) Soil salinization in the study area was severe, and the accumulation of surface salts was obvious, with a mean value of 46,410 mg/kg. The spatial distribution of TSS was predominantly influenced by $Cl^-$, $SO_4^{2-}$, $Na^+ + K^+$, $Mg^{2+}$, and $Ca^{2+}$. (2) Across various soil depths, silt and sand were the primary constituents, with soil fractal dimensions ($D_{soil}$) ranging from 1.91 to 2.76, averaging 2.54, and a poor soil textural structure. The spatial distribution of $D_{soil}$ closely mirrored that of TSS. (3) According to the correlation analysis results, as TSS increased, $D_{soil}$ continued to rise, with an increasing content of clay, while the sand content decreased. Simultaneously, as the soil particles became finer, TSS and $D_{soil}$ also increased, suggesting that sandy loam to silty soils in the study area were more prone to salt accumulation.

**Keywords:** soil salinity; salt ions; particle size distribution of; fractal dimension; Ebinur Lake wetland



Academic Editor: Cezary Kabala

Received: 24 December 2024
Revised: 28 January 2025
Accepted: 28 January 2025
Published: 31 January 2025

**Citation:** Wen, D.; Wang, J.; Ding, J.; Zhang, Z. Distribution Characteristics and Relationship Between Soil Salinity and Soil Particle Size in Ebinur Lake Wetland, Xinjiang. *Land* **2025**, *14*, 297. https://doi.org/10.3390/land14020297



## 1. Introduction

Soil salinization represents a significant challenge to the sustainable ecological functionality of lake wetlands in arid and semi-arid regions [1,2]. The essence of soil salinization lies in the overaccumulation of soluble salts, such as $Na^+$, $K^+$, $Cl^-$, and $SO_4^{2-}$, in the soil [3]. Currently, salinization affects more than 1 billion hectares of land in more than 100 countries, mainly in Africa, Western Asia and Europe, and Western America [4]. In China, salinized soil covers approximately 3690 $km^2$, mainly concentrated in the northern arid zone, the western irrigated zone, and the eastern coastal zone, where the proportion of salinization significantly exceeds the global average.

Soil salinization has become a pressing issue attracting extensive attention from experts both domestically and internationally. Numerous scholars have investigated the causes, characteristics, distribution, and change trends of salinization in arid and semi-arid zones, such as Xinjiang, China [5], the Hetao Irrigation District in Inner Mongolia [6], the coastal area [7], and Europe [8], on the basis of experiments and practical investigations, using methods such as field samples and indoor experiments, and have achieved certain results. For example, Gebremeskel analyzed the planar spatial distribution characteristics of saline soils in Northern Ethiopia and identified discernible patterns in soil salt distribution, providing valuable direction for future research [9]. Additionally, researchers have used correlation analysis to explore the relationships between soil salinity and ions, deepening the understanding of salinity structures. Zheng et al. identified strong correlations between $Cl^-$, $Na^+ + K^+$, $SO_4^{2-}$, $Ca^{2+}$, and $Mg^{2+}$ across soil layers [10]. Li et al. observed that total salt concentration was negatively correlated with $HCO_3^-$ but positively correlated with other ions [11]. Among the anions, $SO_4^{2-}$ and $Cl^-$ showed the strongest correlation, with $Na^+$ being most closely associated with $Cl^-$. At the same time, considerable research was conducted on the spatial heterogeneity of soil salinity. Soil properties such as salinity, water content, and salt ion composition exhibit pronounced spatial and temporal variability. Geostatistical methods, which integrate geographic coordinates with soil data, have proven indispensable for analyzing this heterogeneity. In the 1980s, Burgess et al. introduced the theory of regionalized variables and spatial interpolation methods into the study of spatial heterogeneity of soil salinity to quantify it and push the research forward [12]. Liu et al. used GIS and geostatistical methods to study the spatial variable distribution characteristics of soil features in the Yellow River Delta, and found that the salinity between adjacent soil layers had strong spatial correlation [13]. In terms of research content, domestic and international research on soil salinization has mainly focused on salinization caused by irrigated agriculture [14–18]. However, saline wetlands with unique ecological roles are often overlooked [19] and there are no accurate estimates of current or future salinization of freshwater wetlands in inland and coastal areas on a global scale, which is clearly a pervasive global problem and is expected to worsen over time [20]. In China, wetlands are widespread, with numerous studies focusing on the salinization characteristics of coastal wetlands, including mechanisms and technical methods [21,22]; however, the salinization characteristics of inland lake wetlands differ due to regional environmental variations [1]. In arid and semi-arid regions with low rainfall and high evapotranspiration, lake wetlands are particularly prone to salt accumulation, necessitating urgent attention and research. Wetland salinization is progressing far beyond natural salinity variations [23] and poses a major threat to the sustainability of lake wetland ecosystems. Therefore, addressing soil salinization in these ecosystems is particularly important in arid regions.

The key issue in addressing soil salinization lies in the improvement of soil structure [24]. Essentially, measures to ameliorate saline soils involve regulating soil water and salt movement, promoting the downward leaching of salts, and preventing the upward migration of salts due to evaporation [25,26]. Therefore, understanding the relationship between soil salinity and particle size is crucial. Soil particle size significantly influences the retention and transfer of water, nutrients, air, and heat in the soil [27], and it influences soil permeability, soil water and salt transport, nutrient conversion, and solute migration [28,29], thus affecting soil quality. Numerous factors influence soil salinity accumulation [30]. Soil texture is one of the spatial drivers of soil salinity, characterized by the relative proportions of fine and coarse mineral particles. The size and shape of soil particles affects pore morphology, and the interactions between gravity, cohesion, and capillary forces can affect the movement of water and salts [31]. In assessing soil texture, researchers have found the soil fractal dimension ($D_{soil}$) to be a useful tool for characterizing particle size distribution (PSD)

and soil structure [32,33]. This dimension serves as a quantitative indicator for evaluating soil fertility and degradation [34], reflecting the distribution of coarse and fine particles and their correlation with soil fertility, hydrodynamic properties, and erosion resistance, which are essential for ecological restoration.

During the formation of saline soils, soil particle size plays the role of mediator and carrier, influencing the process of salt stress. Soil salinity is significantly affected by the clay content, with positive correlations between clay and silt fractions and negative correlations with sand [35,36]. Changes in particle size also affect salinity, as alterations in capillary thickness modify water and salt redistribution [37]. In addition, soil texture and its vertical spatial heterogeneity may also greatly affect water and solutes distribution in the soil profile [38]. Zettle indicated that the distribution of soil texture in the vertical profile also significantly affected soil water–salt transport [39]. In arid zone lake wetlands, driven by natural and human factors, the lake water levels decrease, leading to an increase in exposed areas. The salts in these exposed areas migrate horizontally and vertically, accumulating on the surface, which exacerbates the salinization of lake wetlands [40], whereas in the process of water and salt migration, soil particle size, as a critical medium of capillary components, plays a key role in the distribution of salts [41]. However, most studies on soil salinization are limited to the soil surface layer only [42–44], ignoring the characteristics of vertical distribution of salts, whereas a quantitative study of the vertical distribution characteristics of soil salts can accurately obtain the information of potential salinization in the region, which is of great significance in guiding the ecological restoration of wetlands.

Soil texture is the root cause of soil properties, which can vary in properties such as adhesion, water retention, permeability, and ion exchange due to the size of the constituent soil particles and the content of different sized soil particles [45]. Therefore, this study aimed to (i) analyze the distribution characteristics of soil salts/salt ions as well as soil particle size in the vertical profile of Ebinur Lake wetland; (ii) study the relationship between soil salinity and soil particle size in Ebinur Lake wetland; and (iii) analyze the influencing factors of soil salinity, aiming to provide theoretical support for the restoration of the wetland ecosystem of Ebinur Lake.

## 2. Materials and Methods

### 2.1. Study Area

Ebinur Lake Wetland National Reserve is located in the southwest of the Junggar Basin in Xinjiang Uygur Autonomous Region (82°33′–83°53′ E, 44°37′–45°15′ N). Ebinur Lake in the region is the largest saltwater lake in Xinjiang. The region has a typical temperate continental climate, with scarce precipitation (<150 mm/yr), strong evaporation (>2000 mm/yr), and an average annual temperature of about 7.8 °C, making it a typical wetland–desert ecosystem of the temperate arid zone [41]. At the same time, because the wetland is located in the Alashankou gale channel, the wind is always gusty, and its special geographic location makes the area the main source of sand and dust storms in the northern border [46]. Typical soil types in the region are mainly desert soil consisting of piedmont psephitic, salt, and gypsum [47]. The soils are coarse textured and dominated by sandy soils and sandy loams [48]. Due to the special climatic characteristics of the wetland, the low level of the terrain, the soil texture, and the shallow water table, the study area is characterized by severe salinization and the distribution of saline soils over a wide area. Under these environmental conditions, the vegetation in the study area is sparse and dominated by saline plants. Salt-tolerant plants dominated by reeds, pikes, tamarisks, and poplars formed according to the different salt content of the soil [49]. Overall, the high degree of soil salinization and ecological sensitivity [50] of the Ebinur Lake wetland provides a good research example to explore the relationship between salinization and soil

particle size. And this study is of great value for the ecological restoration and promotion of sustainable development in the Ebibur Lake wetland.

### *2.2. Data Collecting and Processing*

The research methods include selecting representative oases, deserts, and ecotones based on the ecological landscape characteristics of the Ebinur Lake wetland, and sampling along the edge of the wetland. As shown in Figure 1, GPS was used for positioning, and 50 sampling points were established. At each profile, four layers were sampled at different depths to reflect the vertical variation in soil salinity, 0–10, 10–20, 20–40, and 40–60 cm, with a total of 200 samples collected. Sampling was conducted in late August 2023. Three soil samples were taken from different soil depths at each sampling point and mixed to form the test sample for that layer. The research technical roadmap was outlined as follows (Figure 2).

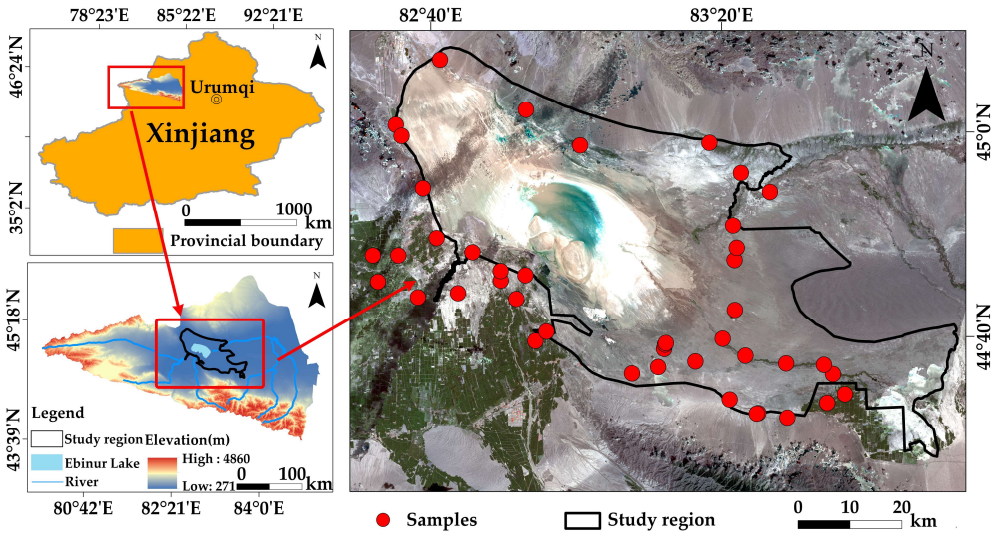


**Figure 1.** Location of study region.

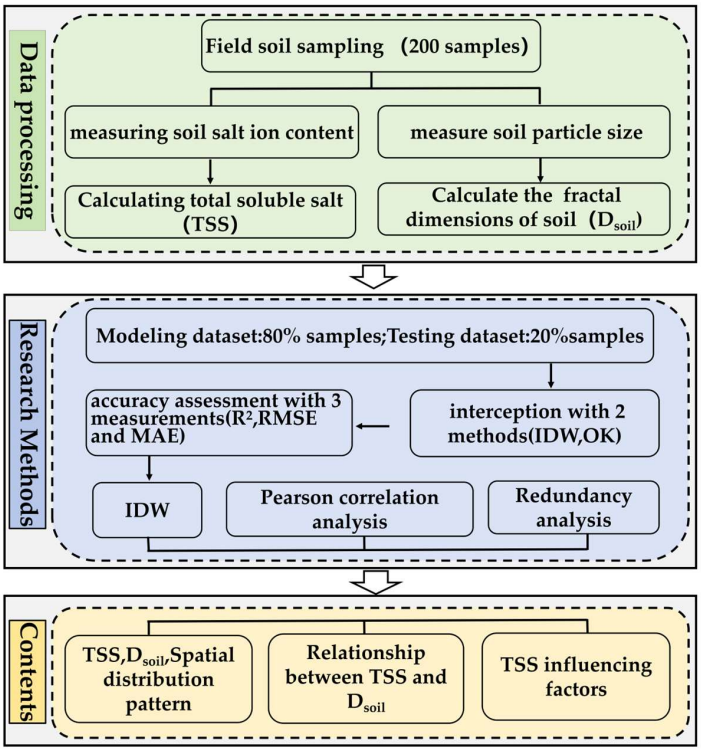


**Figure 2.** Technical flow chart.

#### 2.2.1. Soil Particle Size Measurements

Measurements of the relevant components of soil samples were mainly carried out in laboratories. The soil samples were allowed to air-dry naturally to remove impurities such as grass roots and were ground and passed through a 2 mm sieve before being used for the measurement of soil salt ions and the determination of soil particle size. Soil particle size was measured using a Mastersizer 3000 laser particle size analyzer(Malvern Panalytical, Shanghai, China) to determine the volume fraction of soil particle sizes. Each soil sample was measured three times, and the arithmetic mean was calculated. Soil particle size classification followed the USDA particle size classification standards: clay (<0.002 mm), silt (0.002–0.05 mm), and sand (0.05–2 mm).

#### 2.2.2. Soil Salinity Measurement

Salinity content can be expressed as total soluble salt (TSS) or as soil electrical conductivity (EC) of saturated extract or soil–water suspensions [3]. Whereas EC measurements do not identify the type of salt present in the sample, but only the total cumulative concentration of soluble salts present [51]. Therefore, TSS is used in this paper to represent soil salt content. In general, the choice of the soil–water ratio should be based on the specific purpose, and various ratios can be used, such as 1:1, 1:2, 1:5, and 1:10 for soil-to-water ratios [31,52–54], while 1:2 and 1:5 ratios are more common when testing large numbers of soil samples. Therefore, all things considered, soil samples were used in this study to prepare a soil–water 1:5 soil suspension. The concentrations of $CO_3^{2-}$ and $HCO_3^-$ were determined by dual indicator titration; $Cl^-$ was measured using the $AgNO_3$ method; $SO_4^{2-}$, $Ca^{2+}$, and $Mg^{2+}$ were determined using EDTA; and $Na^+ + K^+$ were measured using the subtraction method. TSS was calculated as the sum of cations and anions [55]. Meanwhile, in this study, saline soil was categorized with reference to the criteria of the Saline and Alkaline Land Specialized Committee of the Soil Society of China [56]. The standards are as follows: when $Cl^-/SO_4^{2-} \geq 2$, it is classified as a chloride type; when $1 \leq Cl^-/SO_4^{2-} < 2$, it is classified as a sulfate–chloride type; when $0.2 \leq Cl^-/SO_4^{2-} < 1$, it is classified as a chloride–sulfate type; and when $Cl^-/SO_4^{2-} < 0.2$, it is classified as a sulfate type.

#### 2.2.3. Soil Fractal Modeling

The fractal dimension of soil ($D_{soil}$) particle size can accurately characterize the distribution characteristics of soil particles and the uniformity of soil texture. Therefore, in this study, $D_{soil}$ was calculated based on the single fractal theory model of soil particle volume derived [57]. The expression formula is as follows:

$$3 - D = \lg\left(\frac{V_{r<R_i}}{V_T}\right) / \lg\left(\frac{R_i}{R_{max}}\right) \quad (1)$$

In the formula, D is the fractal dimension; r is the soil particle size; V ($r < R_i$) is the cumulative volume of particles smaller than a certain size; $V_T$ is the total volume of soil particles; and $R_{max}$ is the upper limit for all particle sizes, numerically the maximum particle size. To calculate, first determine the slope of the least squares fitted line of $\lg\left(\frac{V_{r<R_i}}{V_T}\right)$ and $\lg\left(\frac{R_i}{R_{max}}\right)$, which equals 3–D, and then derive the fractal dimension D.

#### 2.2.4. Inverse Distance Weighting

The inverse distance weighting (IDW) interpolation method is primarily based on the first law of geography, which determines the value of the interpolation point based on the inverse of the distance between the interpolation point and the sample points [58]. In other words, the farther the interpolation point is from the sample points, the smaller the

influence, and vice versa. The main advantage of this method is its high computational efficiency and simple structure. The formula is as follows:

$$\hat{z}(s_0) = \sum_{i=1}^{N} (\lambda_i) z(s_i) \tag{2}$$

$$\lambda_i = \frac{1}{(D_i)^p} \left[ \sum_{i=1}^{N} \frac{1}{(D_i)^p} \right]^{-1} \tag{3}$$

In the formula, $\hat{z}(s_0)$ represents the estimated attribute value at the point $s_0$, N is the sample size, $\lambda_i$ is the weight, $z(s_i)$ is the attribute value at the sample point $s_i$, $D_i$ is the distance between the sample point at point i and the estimation point, and p is the power exponent, typically defined as 2.

#### 2.2.5. Ordinary Kriging

The essence of the kriging method is to use the observed data of the regionalized variables at the sampling points to perform an unbiased estimation of the data at the interpolation point, with the most commonly used being the ordinary kriging (OK) method [59] where the data at an interpolation point are estimated as a linear combination of the observed values from the sample points. The general formula is as follows:

$$Z(x_0) = \sum_{i=1}^{N} \lambda_1 Z(x_i) \tag{4}$$

In the equation, $Z(x_0)$ represents the value of the predicted unknown point; $Z(x_i)$ represents the value of the known sample points surrounding the predicted unknown sample point; N is the number of known sample points; and λ is the weight of the i-th sample point.

#### 2.2.6. Statistical and Geostatistical Analysis

Descriptive statistical analysis was conducted on salinity data and particle size data using SPSS 25.0, and the minimum, maximum, mean, standard deviation (SD), and coefficient of variation (CV) were determined for all datasets to analyze the vertical distribution characteristics of soil salinity and particle size. The coefficient of variation is an indicator used to measure the degree of data variation. Based on the CV values, variations are generally categorized as low (CV < 10%), medium (CV between 10% and 100%), and high (CV > 100%). Then, SPSS was used to perform Pearson correlation analysis, Origin 2021 was used to plot correlation heatmaps, and the relationship between soil salinity and particle size was investigated. Finally, redundancy analysis [60] was used to investigate the influencing factors of salinity.

## 3. Results

### *3.1. Characterization of Soil Salinity/Salt Ion Distribution*

#### 3.1.1. Vertical Distribution Characteristics of Total Soil Salinity

The statistical description of TSS at various soil depths within the study area is presented in Table 1. The overall salt content in the study area was relatively high, with variations in TSS at different soil depths. TSS decreases with increasing soil depth, with the maximum TSS value at the soil surface (0–10 cm), reaching 143,790 mg/kg (Figure 3). The surface layer salt accumulation in the study area was evident. The coefficient of variation (CV) of the surface layer was 77%, significantly higher than that of other soil layers. As shown in Table 1, the salinity data at different soil depths all fall within the

medium variability range. The CV decreases with increasing soil depth, in the order of 0–10 > 10–20 > 20–40 > 40–60 cm.

**Table 1.** Statistical characteristics of total soluble salt content/salt ions at different soil depths. Unit: mg/kg.

| Soil Depth (cm) | Statistic | $CO_3^{2-}$ | $HCO_3^-$ | $Cl^-$ | $SO_4^{2-}$ | $Ca^{2+}$ | $Mg^{2+}$ | $Na^+ + K^+$ | TSS |
|---|---|---|---|---|---|---|---|---|---|
| 0–10 | Min | 0 | 24 | 71 | 960 | 120 | 100 | 700 | 7805 |
| | Max | 340 | 900 | 77,810 | 40,220 | 4850 | 5190 | 51,350 | 143,790 |
| | Mean | 86 | 353 | 18,533 | 10,458 | 2182 | 1189 | 13,604 | 46,406 |
| | SD | 114 | 182 | 21,035 | 5349 | 1259 | 1382 | 12,929 | 35,877 |
| | CV | 132 | 51 | 114 | 51 | 58 | 116 | 95 | 77 |
| 10–20 | Min | 0 | 50 | 70 | 2300 | 100 | 80 | 810 | 4490 |
| | Max | 380 | 710 | 43,040 | 19,100 | 3830 | 5870 | 24,940 | 88,400 |
| | Mean | 60 | 330 | 6100 | 9500 | 1560 | 620 | 6310 | 24,500 |
| | SD | 100 | 160 | 8230 | 2590 | 1100 | 870 | 4930 | 15,090 |
| | CV | 163 | 47 | 135 | 27 | 71 | 139 | 78 | 62 |
| 20–40 | Min | 0 | 50 | 70 | 1820 | 100 | 120 | 30 | 3930 |
| | Max | 430 | 970 | 24,990 | 12,380 | 3190 | 1710 | 17,270 | 54,290 |
| | Mean | 70 | 330 | 4480 | 7730 | 1210 | 520 | 4910 | 19,250 |
| | SD | 110 | 170 | 5520 | 2760 | 1110 | 400 | 3850 | 11,080 |
| | CV | 155 | 50 | 123 | 36 | 91 | 78 | 79 | 58 |
| 40–60 | Min | 0 | 20 | 70 | 1340 | 110 | 30 | 320 | 3970 |
| | Max | 310 | 780 | 26,940 | 14,210 | 3230 | 1850 | 19,370 | 56,710 |
| | Mean | 70 | 300 | 4040 | 7980 | 1030 | 530 | 4940 | 18,880 |
| | SD | 100 | 130 | 5520 | 2540 | 1100 | 380 | 3640 | 10,450 |
| | CV | 137 | 44 | 137 | 32 | 107 | 72 | 74 | 55 |

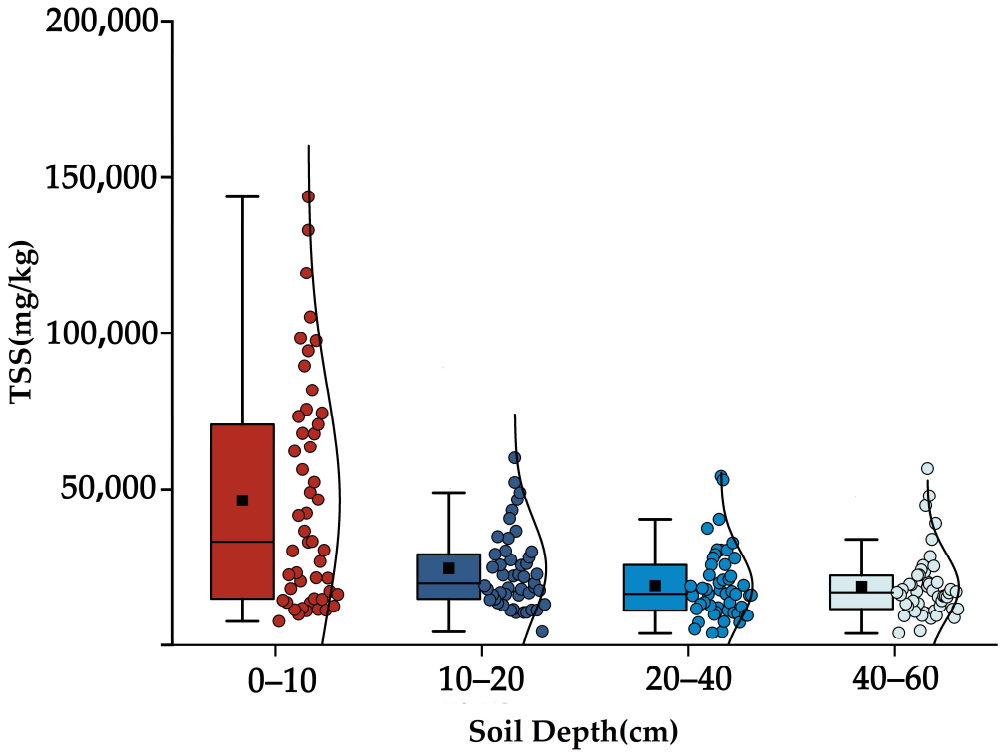


**Figure 3.** A box plot of TSS at different soil depths. The box shape represents the interquartile range. The 75th percentile is at the top of the box and the 25th percentile is at the bottom of the box; the horizontal line in the center represents the median soil salinity for each layer, and the small box in the box represents the mean. The short horizontal lines extending from the top and bottom of the box represent the maximum and minimum values of the data.

The relationship of TSS at different soil depths was investigated based on Pearson's correlation analysis, and as shown in Table 2, the TSS between different soil layers showed a significant correlation, with the correlation coefficients ranging from 0.579 to 0.843. The correlation coefficients between adjacent soil layers, i.e., 0–10 and 10–20, 10–20 and 20–40, and 20–40 and 40–60, were 0.611, 0.669, and 0.843, respectively. The correlations were all significant at the 0.01 level, which indicated that the soil salinity at a particular depth was determined by the salinity values of the neighboring soil layers. Therefore, this study quantitatively investigated the relationship of different soil depths and TSS by establishing multiple linear regression equations. The regression equations were shown as a, b, c, and d. Analysis of variance and significance testing of regression coefficients were conducted for the established regression equations; the results indicated significant correlation in the regression equations.

$$TS_{0-10} = 0.854TS_{10-20} + 0.693TS_{20-40} + 0.592TS_{40-60} + 0.976 \quad R^2 = 0.448 \quad F = 12.421 \quad Sig = 0.00 \tag{5}$$

$$TS_{10-20} = 0.131TS_{0-10} + 0.487TS_{20-40} + 0.214TS_{40-60} + 5.017 \quad R^2 = 0.552 \quad F = 16.742 \quad Sig = 0.00 \tag{6}$$

$$TS_{20-40} = 0.030TS_{0-10} + 0.138TS_{10-20} + 0.709TS_{40-60} + 1.082 \quad R^2 = 0.748 \quad F = 45.528 \quad Sig = 0.00 \tag{7}$$

$$TS_{40-60} = 0.025TS_{0-10} + 0.059TS_{10-20} + 0.692TS_{20-40} + 2.933 \quad R^2 = 0.723 \quad F = 40.049 \quad Sig = 0.00 \tag{8}$$

**Table 2.** Relationship of soil salinity between different depths based on Pearson correlation analysis.

| Soil Depth (cm) | 0–10 | 10–20 | 20–40 | 40–60 |
|---|---|---|---|---|
| 0–10 | 1 | | | |
| 10–20 | 0.611 ** | 1 | | |
| 20–40 | 0.600 ** | 0.669 ** | 1 | |
| 40–60 | 0.579 ** | 0.629 ** | 0.843 ** | 1 |

** Correlation is significant at 0.01 level (two-tailed).

### 3.1.2. Characteristics of Vertical Distribution of Salt Ions and Major Saline Soil Types

As can be seen in Figure 4, in conjunction with the depth of soil sampling, the overall salt ion content was highest in the surface layer, second highest in the second layer, and lowest in the fourth layer. The anions were $Cl^- > SO_4^{2-} > HCO_3^- > CO_3^{2-}$ and the cations were $Na^+ + K^+ > Ca^{2+} > Mg^{2+}$ in the soil surface. This showed that the major anions in the study region were $Cl^-$ and $SO_4^{2-}$ and the major cations were dominated by $Na^+ + K^+$. The coefficients of variation in $Cl^-$, $CO_3^{2-}$, and $Mg^{2+}$ among all the ions were more than 100%, which were highly variable ions, while the other ions were of medium variation.

Correlation analysis between soil salt ions can help to reveal the synergistic migration of salt ions in soil [61]; therefore, this study was conducted using a Pearson correlation analysis between TSS and salt ions using SPSS 25.0. From the surface to the deeper layers, the correlation between soil salinity and salt ions showed significant differences. As shown in Figure 5, TSS showed non-significant correlation with both $HCO_3^-$ in 0–60 cm soil layer; non-significant correlation with $CO_3^{2-}$ in 20–40,40–60, and significant correlation in this soil layer; and significant correlation with $SO_4^{2-}$ in all but 0–10 cm soil layer. In addition to this, TSS showed significant correlation with all other ions, with the largest correlation coefficients with $Cl^-$, $Na^+ + K^+$, all of which had correlation coefficients above 0.9. It indicates that soil salinity is mainly associated with $Cl^-$, $SO_4^{2-}$, $CO_3^{2-}$, $Ca^{2+}$, $Mg^{2+}$, $Na^+$

+ $K^+$. From the results of the correlation of salt ions with each other, $Cl^-$ and $Na^+ + K^+$ showed highly significant correlation with correlation coefficients above 0.9 in all soil layers. In addition, in 0–10 cm $CO_3^{2-}$ vs. $Na^+ + K^+$; $Cl^-$ vs. $Ca^{2+}$; in 10–20 cm $CO_3^{2-}$ vs. $Mg^{2+}$; $Cl^-$ vs. $Mg^{2+}$; in 20–40 cm $CO_3^{2-}$ vs. $Ca^{2+}$; $SO_4^{2-}$ with $Ca^{2+}$; $SO_4^{2-}$ with $Na^+ + K^+$; and $CO_3^{2-}$ with $Ca^{2+}$; $Cl^-$ with $Mg^{2+}$; $SO_4^{2-}$ with $Na^+ + K^+$ in 40–60 cm showed highly significant correlation. Overall, the correlations between TSS and $Cl^-$ and $Na^+ + K^+$, as well as between $Cl^-$ and $Na^+ + K^+$, were high, suggesting that $Na^+ + K^+$ and $Cl^-$ have the strongest synergistic migration ability.

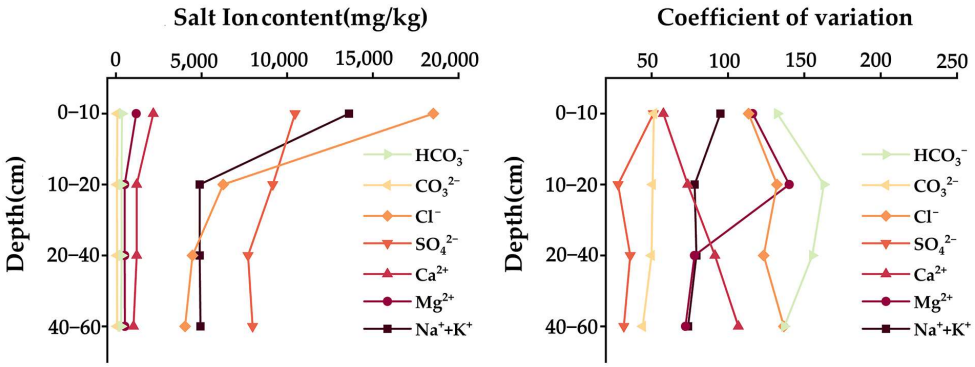


**Figure 4.** Vertical variation in soil anions and cations at different soil depths.

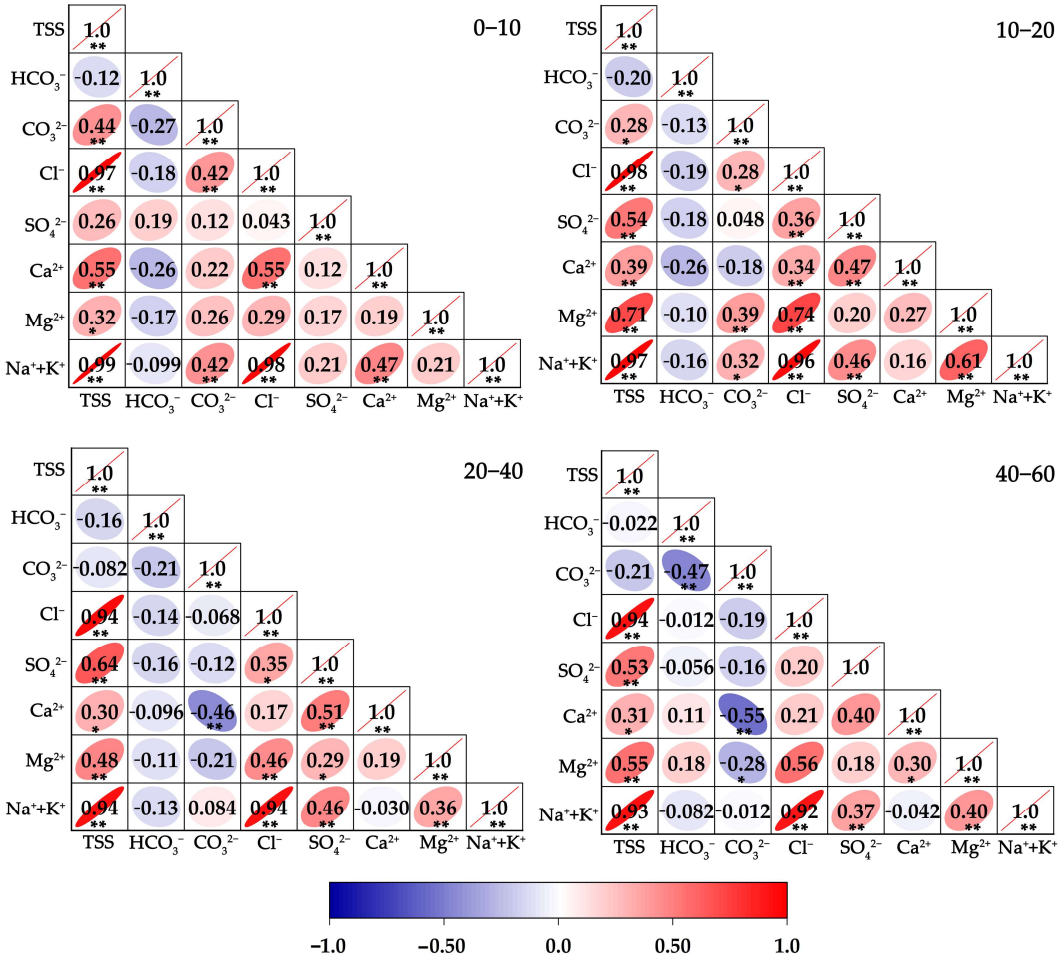


**Figure 5.** Correlation analysis between TS and eight ions.

In order to further explore the main types of salts in each soil layer, in this study, we classified salinized soils according to the standards of the Saline Soil Specialized Committee

of the Soil Society of China. According to the results in Table 3, the degree of soil salinity in the study area was relatively high, with $Cl^-$ content in the surface layer accounting for approximately 36% of the total ion content. However, the proportion significantly decreases at other soil depths. Therefore, the surface saline soil was mainly of the chloride type, while other soil layers predominantly exhibited chloride–sulfate and sulfate types. Moderately saline soils, heavily saline soils, and saline soils in the study area accounted for 4, 24, and 74%, respectively, indicating that the study area had a high degree of salinization, which was mainly dominated by chloride-type salinization, with good a solubility of chloride.

**Table 3.** Classification of saline soil types and degree of salinization in Ebinur Lake wetland.

| **Soil Depth (cm)** | **$2 \leq Cl^-/SO_4^{2-}$ (%) Chloride** | **$1 \leq Cl^-/SO_4^{2-} < 2$(%) Sulfate–Chloride** | **$0.2 \leq Cl^-/SO_4^{2-} < 221$(%) Chloride–Sulfate** | **$Cl^-/SO_4^{2-} < 20.2$(%) Sulfate** |
|---|---|---|---|---|
| 0–10 | 36.00 | 12.00 | 24.00 | 28.00 |
| 10–20 | 4.00 | 18.00 | 38.00 | 40.00 |
| 20–40 | 4.00 | 12.00 | 44.00 | 40.00 |
| 40–60 | 2.00 | 16.00 | 40.00 | 42.00 |
| **Grading of soil salinization** | **Chloride** | **Sulfate–chloride** | **Chloride–sulfate** | **Sulfate** |
| Non-saline Criteria Value | $TSS_{0–10} < 1500$ | $TSS_{0–10} < 2000$ | $TSS_{0–10} < 2500$ | $TSS_{0–10} < 3000$ |
| Light salinized Criteria Value | $1500 < TSS_{0–10} < 3000$ | $2000 < TSS_{0–10} < 3000$ | $2500 < TSS_{0–10} < 4000$ | $3000 < TSS_{0–10} < 6000$ |
| Moderate salinized Criteria Value | $3000 < TSS_{0–10} < 5000$ | $3000 < TSS_{0–10} < 6000$ | $4000 < TSS_{0–10} < 7000$ 2% | $6000 < TSS_{0–10} < 10{,}000$ 2% |
| Heavy salinized Criteria Value | $5000 < TSS_{0–10} < 8000$ | $6000 < TSS_{0–10} < 10{,}000$ | $7000 < TSS_{0–10} < 12{,}000$ 4% | $10{,}000 < TSS_{0–10} < 20{,}000$ 20% |
| Salinized soil Criteria | $TSS_{0–10} \geq 8000$ 36% | $TSS_{0–10} \geq 10{,}000$ 12% | $TSS_{0–10} \geq 12{,}000$ 20% | $TSS_{0–10} \geq 20{,}000$ 6% |

The percentages in the table are ratios of the corresponding sampling site to the total sampling site TSS, and the subscripts 0–10 indicate the total soluble salt (mg/kg) at soil depths of 0–10 cm. And Bold font indicates table header.

#### 3.1.3. Characterization of Spatial Distribution of Soil Salinity

Geostatistical analyses play a critical role in decision-making processes related to environmental remediation, monitoring, and land management [62]. Various interpolation methods were employed to predict the spatial distribution of soil salinity, including IDW and OK [63]. However, different interpolation methods often yield varying results. To achieve a more accurate understanding of the spatial distribution characteristics of TSS and salt ions, this study compared two widely used interpolation methods for soil salinity. The objective is to identify the most suitable interpolation method for the study area. Salinity data were interpolated in ArcGIS 10.6 using IDW and OK, and 80% (40 samples) were used as the training set, and 20% (10 samples) were used as the testing set. The accuracy and reliability of spatial interpolation were evaluated by three metrics: $R^2$, RMSE, and MAE. As shown in Table 4, two spatial interpolation methods exhibited significant differences. Except for the $HCO_3^-$, the $R^2$, RMSE, and MAE of other ions were superior to those of OK, indicating that IDW achieved better fitting performance for the test data than OK. Overall, the IDW interpolation method exhibited smaller errors, higher accuracy, and greater stability, making it more suitable for salinity interpolation in the Ebinur Lake wetland compared to OK. It can more effectively reveal the spatial distribution of soil salinity and soil particle size. Furthermore, based on interpolation methods employed by

other researchers in the Ebinur Lake wetland [64], this study selected IDW as the spatial interpolation method.

In this paper, the spatial distribution maps of TSS and each ion from 0 to 10 cm were obtained by spatial interpolation using IDW. As shown in Figure 6, the spatial distribution characteristics of TSS and salt ions are more similar, and the overall distribution is more dispersed. The high value areas of TSS were mainly distributed in the periphery of Lake Ebey, such as the northwest and southwest sides of the lake, as well as the southeast side of the lake. The spatial distributions of TSS were roughly the same as those of $Cl^-$, $SO_4^{2-}$, and $Na^+ + K^+$; and the trend of spatial distribution was opposite to that of $HCO_3^-$. And from the comparison between ions, it can be seen that the spatial distribution of $Cl^-$ and $Na^+ + K^+$ is extremely similar; contrary to the trend of the spatial distribution of $HCO_3^-$, the spatial distribution of $SO_4^{2-}$ is more similar to that of $Ca^{2+}$ and $Mg^{2+}$.

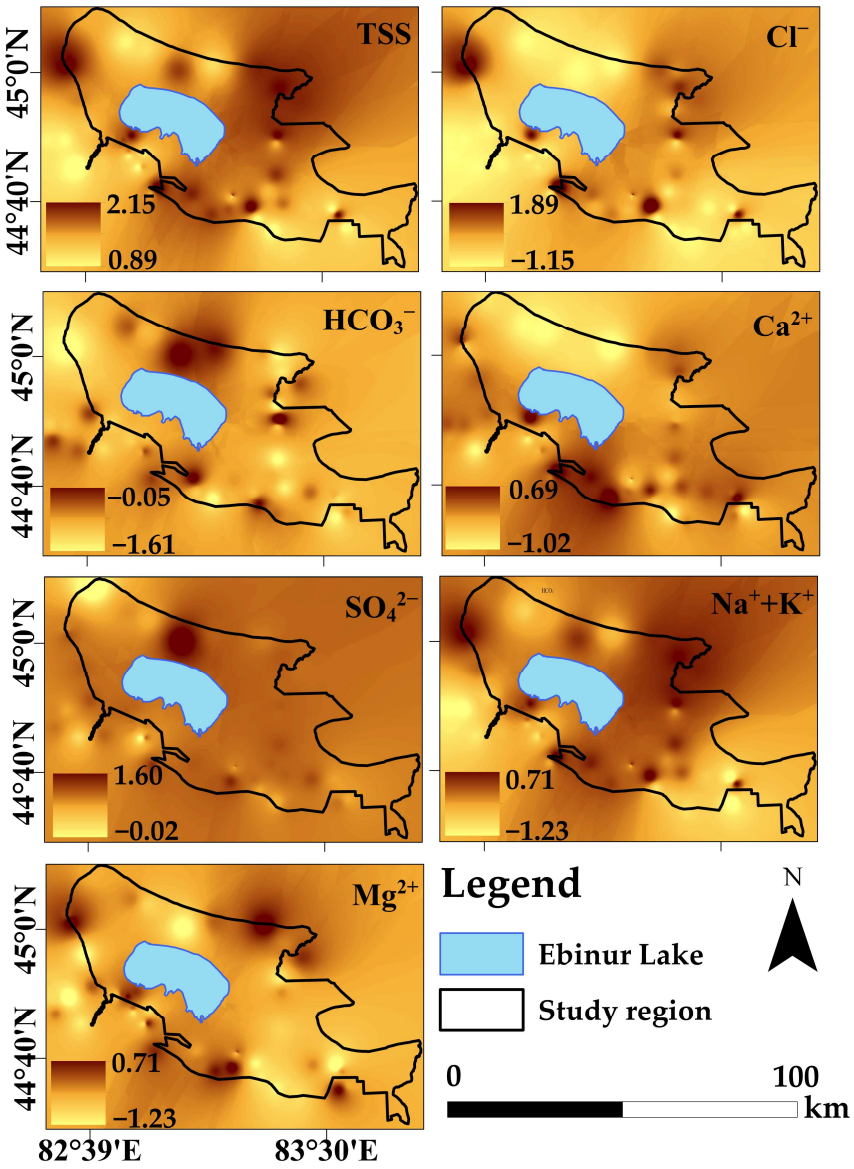


**Figure 6.** Spatial interpolation of TSS and salt ions (0–10 cm).

**Table 4.** Validation and comparison of 0–10 cm IDW and OK interpolation methods. Unit: $10^3$ mg/kg.

| Variable | Method | $R^2$ | RMSE | MAE |
|---|---|---|---|---|
| TSS | OK | 0.43 | 7.31 | 6.36 |
| | IDW | 0.56 | 6.71 | 5.31 |
| $HCO_3^-$ | OK | 0.35 | 0.04 | 0.03 |
| | IDW | 0.34 | 0.03 | 0.03 |
| $Cl^-$ | OK | 0.40 | 3.99 | 3.43 |
| | IDW | 0.68 | 3.09 | 2.53 |
| $SO_4^{2-}$ | OK | 0.78 | 2.08 | 1.37 |
| | IDW | 0.80 | 1.31 | 0.88 |
| $Ca^{2+}$ | OK | 0.43 | 0.26 | 0.21 |
| | IDW | 0.59 | 0.24 | 0.21 |
| $Mg^{2+}$ | OK | 0.53 | 0.26 | 0.21 |
| | IDW | 0.59 | 0.24 | 0.20 |
| $Na^+ + K^+$ | OK | 0.54 | 2.50 | 2.16 |
| | IDW | 0.62 | 1.45 | 1.84 |
| $D_{soil}$ | OK | 0.44 | 0.04 | 0.04 |
| | IDW | 0.50 | 0.05 | 0.04 |
| Clay | OK | 0.55 | 2.20 | 1.77 |
| | IDW | 0.71 | 2.10 | 1.68 |
| Silt | OK | 0.53 | 19.19 | 16.15 |
| | IDW | 0.53 | 18.85 | 15.67 |
| Sand | OK | 0.43 | 21.28 | 16.15 |
| | IDW | 0.53 | 20.81 | 17.03 |

### *3.2. Statistical Description and Spatial Distribution Characteristics of Soil Particle Size*

Descriptive statistics were analyzed for PSD at different soil depths in the Ebinur Lake wetland, and the results are shown in Table 5. The soil particles at different depths in the study area were primarily composed of silt and sand, with the maximum volume fraction of sand reaching 97.6% and the minimum volume fraction of clay being 0.03%. At the soil surface, sand was the most common category (49.04%), followed by silt (45.32%) and clay (5.64%). At other soil depths, the silt content ranges from 39.47 to 40.64%, while the sand content ranges from 54.12 to 55.46%. From the perspective of variability, the variability in clay content was the most pronounced, followed by silt, with sand showing the least variability. A triangular classification diagram of the top 50 samples was created according to the USDA soil texture classification (Figure S1). The surface soil texture mainly consists of sandy soil, sandy loam, loamy sand, and silty loam. The soil textures at other depths generally include sandy soil, sandy loam, loamy sand, loam, silty loam, and silt loam (Table S1). The characteristics of these soil types include a high sand content, low clay and silt content, good permeability, and poor water retention [65].

In reality, the distribution of soil types is complex and intricate, making it difficult to determine the distribution characteristics and texture uniformity of soil particles in the study area. Therefore, this study used the measured particle size results and the IDW interpolation method to obtain the spatial distribution of surface layer PSD and $D_{soil}$ in the Ebinur Lake wetland (Figure 7). Regarding surface layer PSD, the volume fraction of clay particles was generally relatively low. It was mainly distributed in the northwest corner of Ebinur Lake, the narrow strip on the southwest side of Ebinur Lake (mainly referring to the lower reaches of the Jing River riparian zone), and the northeast side (mainly with some high value points in the lower reaches of the Kuitun River). The spatial distribution trend of silt content was similar to that of clay particles. In contrast, the spatial distribution of the sand particles was exactly opposite to that of the clay particles, with lower volume fractions of sand in some areas on the northwest, southwest, and northeast sides of Ebinur Lake. Generally, the spatial distribution trend showed a higher sand content on the southeast side of the lake compared to the northwest side.

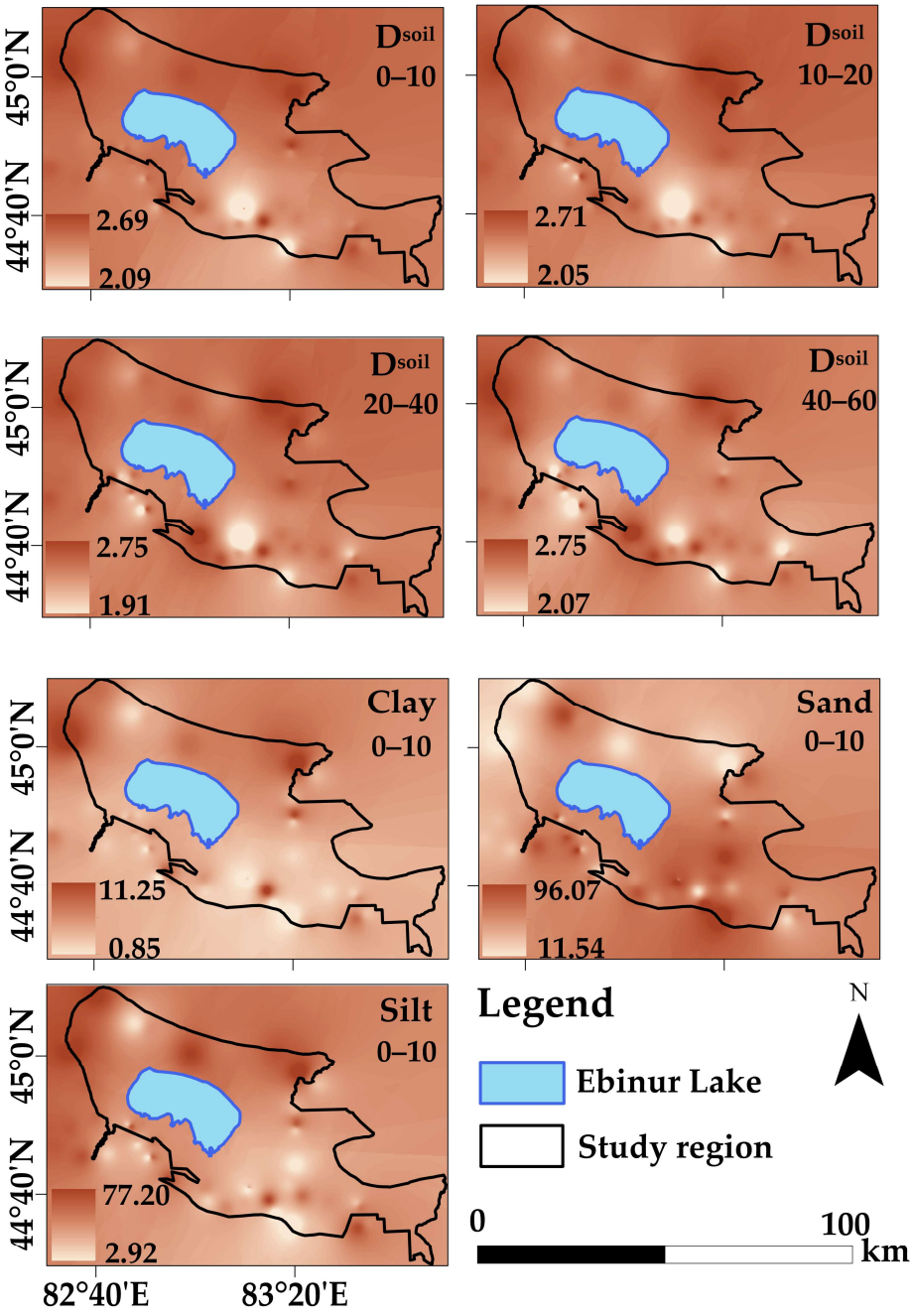


**Figure 7.** Spatial distribution of PSD (0–10) and spatial distribution of $D_{soil}$ at different soil depths.

**Table 5.** Statistical characteristics of soil particle size in each layer.

| Soil Depth (cm) | Minimum | Maximum | Average Value | Standard Deviation | Coefficient of Variation | Skewness | Kurtosis |
|---|---|---|---|---|---|---|---|
| Clay (%) | | | | | | | |
| 0–10 | 0.10 | 11.26 | 5.64 | 2.48 | 0.44 | 0.49 | 0.11 |
| 10–20 | 0.11 | 13.98 | 5.07 | 2.99 | 0.59 | 0.78 | 0.80 |
| 20–40 | 0.03 | 16.99 | 5.04 | 3.64 | 0.72 | 1.08 | 1.40 |
| 40–60 | 0.15 | 18.00 | 5.23 | 3.71 | 0.71 | 1.12 | 1.63 |
| Silt (%) | | | | | | | |
| 0–10 | 2.92 | 77.24 | 45.32 | 19.18 | 0.42 | −0.33 | −0.73 |
| 10–20 | 2.52 | 78.68 | 39.47 | 20.96 | 0.53 | 0.02 | −1.11 |
| 20–40 | 1.94 | 79.41 | 39.51 | 22.97 | 0.58 | −0.03 | −1.28 |
| 40–60 | 2.35 | 80.82 | 40.64 | 21.90 | 0.54 | −0.09 | −1.10 |

**Table 5.** *Cont.*

| Soil Depth (cm) | Minimum | Maximum | Average Value | Standard Deviation | Coefficient of Variation | Skewness | Kurtosis |
|---|---|---|---|---|---|---|---|
| Sand (%) | | | | | | | |
| 0–10 | 11.50 | 96.19 | 49.04 | 21.30 | 0.43 | 0.27 | −0.64 |
| 10–20 | 9.88 | 96.77 | 55.46 | 23.48 | 0.42 | −0.06 | −0.96 |
| 20–40 | 9.23 | 97.60 | 55.45 | 25.90 | 0.47 | −0.01 | −1.18 |
| 40–60 | 8.78 | 96.94 | 54.12 | 24.79 | 0.46 | 0.04 | −1.03 |

The $D_{soil}$ at different soil depths in the study area ranged from 1.91 to 2.76 with a mean value of 2.54. The spatial distribution of $D_{soil}$ was extremely similar to that of clay and silt. At the same time, the spatial distribution of $D_{soil}$ at different soil depths remained generally consistent. Overall, $D_{soil}$ exhibited an increase with increasing content of clay, silt; a decrease with decreasing sand content; and an increase with increasing content of TSS (Figure S2).

### *3.3. Correlation Analysis Between Soil Salts/Ions and Soil Particle Size*

#### 3.3.1. Correlation Between Soil Salts/Ions and Soil Particle Size

To accurately reflect the relationship between soil fractal dimension and soil salinization, this study first averaged the TSS and $D_{soil}$ of all soil depths in the study area to analyze the spatial distribution characteristics of soil fractal dimension and salinity. Secondly, Pearson correlation analysis was performed on TSS, $D_{soil}$, and salt ions to analyze the relationship between PSD and soil salinization at soil depth from 0 to 60 cm. As shown in Figure 8a, the trend line of $D_{soil}$ in the green line at the Ebinur Lake wetland was concave, showing a decreasing-then-increasing trend overall, with a general decreasing trend in the blue line. The trend line of TSS in the green line was also concave, showing a decreasing-then-increasing pattern, while the blue line showed a linear decreasing trend (Figure 8b). Overall, $D_{soil}$ and TSS follow the same trend.

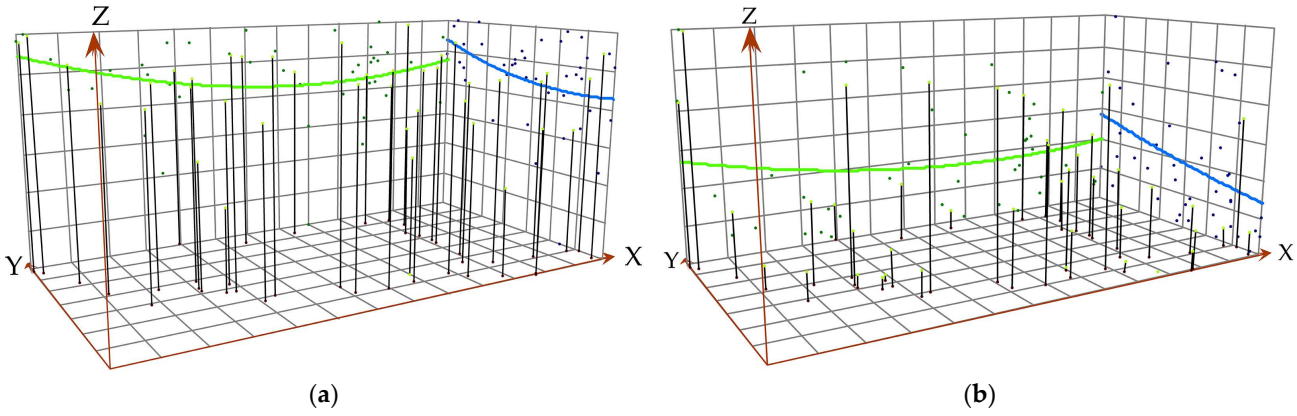


(**a**) (**b**)

**Figure 8.** Spatial distribution of soil fractal dimensions, salinity at edge of Ebinur Lake wetland. (**a**) Soil fractal dimension, $D_{soil}$; (**b**) total soluble salt, TSS.

Table 6 showed that TSS had a significant positive correlation with $D_{soil}$, clay, and silt, and a negative correlation with sand. The strength of the correlation was TSS-Clay > TSS-Silt > TSS-Sand. In terms of salt ions correlating with each other, $CO_3^{2-}$, $HCO_3^-$, and $SO_4^{2-}$ were significantly uncorrelated with $D_{soil}$ in all layers, whereas $Cl^-$ was the opposite, showing a high correlation. $Ca^{2+}$ and $D_{soil}$ among cations showed a gradual increase in correlation with increasing soil depth, while $Na^+ + K^+$ changed in the opposite trend. The trend of the correlation between $Mg^{2+}$ and $D_{soil}$ was mainly "S" shaped. In summary, it showed that $Cl^-$ and $Na^+ + K^+$ were the overwhelmingly dominant ions in

the migration of ions in the bottom–up process. Clay showed non-significant negative correlation with $HCO_3^-$ in all soil layers; negative correlation with $CO_3^{2-}$ in the 20–40 cm layer; except for this, clay was positively correlated with all other ions. Silt was the same as clay. In sand, $CO_3^{2-}$ and $HCO_3^-$ showed a positive correlation with sand except in some soil layers, which was the opposite of the case for both particle sizes of clay/silt, and all the rest of the ions showed a negative correlation with sand.

**Table 6.** Pearson's correlation analysis of salts/salt ions and soil particle size in Ebinur Lake wetland.

| | $D_{soil}$ | | CLAY | | SILT | | SAND | |
|---|---|---|---|---|---|---|---|---|
| **0–10** | **R** | **Sig** | **R** | **Sig** | **R** | **Sig** | **R** | **Sig** |
| TSS | 0.420 ** | 0.002 | 0.582 ** | 0.000 | 0.440 ** | 0.001 | −0.464 ** | 0.001 |
| $CO_3^{2-}$ | 0.260 | 0.068 | 0.327 * | 0.020 | 0.295 * | 0.038 | −0.304 * | 0.032 |
| $HCO_3^-$ | −0.073 | 0.617 | −0.059 | 0.683 | −0.076 | 0.598 | 0.076 | 0.602 |
| $Cl^-$ | 0.395 ** | 0.004 | 0.568 ** | 0.000 | 0.410 ** | 0.003 | −0.435 ** | 0.002 |
| $SO_4^{2-}$ | 0.171 | 0.234 | 0.142 | 0.326 | 0.201 | 0.162 | −0.197 | 0.170 |
| $Ca^{2+}$ | 0.292 * | 0.040 | 0.174 | 0.227 | 0.288 * | 0.043 | −0.279 * | 0.050 |
| $Mg^{2+}$ | 0.182 | 0.206 | 0.198 | 0.168 | 0.283 * | 0.046 | −0.278 | 0.051 |
| $Na^+ + K^+$ | 0.402 ** | 0.004 | 0.590 ** | 0.000 | 0.413 ** | 0.003 | −0.441 ** | 0.001 |
| 10–20 | | | | | | | | |
| TSS | 0.448 ** | 0.001 | 0.550 ** | 0.000 | 0.418 ** | 0.002 | −0.444 ** | 0.001 |
| $CO_3^{2-}$ | 0.233 | 0.103 | 0.295 * | 0.037 | 0.207 | 0.149 | −0.222 | 0.121 |
| $HCO_3^-$ | 0.015 | 0.920 | −0.052 | 0.719 | 0.108 | 0.453 | −0.090 | 0.533 |
| $Cl^-$ | 0.447 ** | 0.001 | 0.568 ** | 0.000 | 0.450 ** | 0.001 | −0.474 ** | 0.001 |
| $SO_4^{2-}$ | 0.182 | 0.207 | 0.154 | 0.285 | 0.046 | 0.753 | −0.060 | 0.677 |
| $Ca^{2+}$ | 0.357 * | 0.011 | 0.316 * | 0.025 | 0.280 * | 0.049 | −0.290 * | 0.041 |
| $Mg^{2+}$ | 0.266 | 0.062 | 0.349 * | 0.013 | 0.342 * | 0.015 | −0.350 * | 0.013 |
| $Na^+ + K^+$ | 0.398 ** | 0.004 | 0.519 ** | 0.000 | 0.376 ** | 0.007 | −0.401 ** | 0.004 |
| 20–40 | | | | | | | | |
| TSS | 0.493 ** | 0.000 | 0.703 ** | 0.000 | 0.476 ** | 0.000 | −0.521 ** | 0.000 |
| $CO_3^{2-}$ | −0.083 | 0.565 | −0.170 | 0.238 | −0.205 | 0.154 | 0.205 | 0.152 |
| $HCO_3^-$ | −0.001 | 0.992 | −0.119 | 0.410 | 0.069 | 0.632 | −0.045 | 0.757 |
| $Cl^-$ | 0.485 ** | 0.000 | 0.728 ** | 0.000 | 0.534 ** | 0.000 | −0.576 ** | 0.000 |
| $SO_4^{2-}$ | 0.274 | 0.054 | 0.315 * | 0.026 | 0.120 | 0.407 | −0.150 | 0.297 |
| $Ca^{2+}$ | 0.375 ** | 0.007 | 0.432 ** | 0.002 | 0.362 ** | 0.010 | −0.382 ** | 0.006 |
| $Mg^{2+}$ | 0.265 | 0.063 | 0.267 | 0.060 | 0.318 * | 0.024 | −0.319 * | 0.024 |
| $Na^+ + K^+$ | 0.393 ** | 0.005 | 0.609 ** | 0.000 | 0.383 ** | 0.006 | −0.425 ** | 0.002 |
| 40–60 | | | | | | | | |
| TSS | 0.386 ** | 0.006 | 0.607 ** | 0.000 | 0.421 ** | 0.002 | −0.462 ** | 0.001 |
| $CO_3^{2-}$ | −0.198 | 0.168 | −0.322 * | 0.023 | −0.323 * | 0.022 | 0.334 * | 0.018 |
| $HCO_3^-$ | 0.120 | 0.406 | 0.116 | 0.423 | 0.175 | 0.224 | −0.172 | 0.233 |
| $Cl^-$ | 0.458 ** | 0.001 | 0.685 ** | 0.000 | 0.494 ** | 0.000 | −0.539 ** | 0.000 |
| $SO_4^{2-}$ | −0.020 | 0.891 | 0.053 | 0.715 | −0.006 | 0.965 | −0.002 | 0.988 |
| $Ca^{2+}$ | 0.401 ** | 0.004 | 0.421 ** | 0.002 | 0.425 ** | 0.002 | −0.438 ** | 0.001 |
| $Mg^{2+}$ | 0.378 ** | 0.007 | 0.453 ** | 0.001 | 0.538 ** | 0.000 | −0.543 ** | 0.000 |
| $Na^+ + K^+$ | 0.265 | 0.062 | 0.496 ** | 0.000 | 0.280 * | 0.049 | −0.321 * | 0.023 |

#### 3.3.2. Percentage of Total Salts/Salt Ions in Different Soil Textures

To further explore the relationship between TSS and PSD, soil texture types at different depths were classified according to the USDA soil texture classification standards, and the relationship between soil salinity and particle size distribution in different soil textures was examined. According to Table 7, the number of samples for sandy soil and loamy sand, sandy loam and loam, and silty loam and silt in the study area were 55, 78, and 67, respectively, with the total proportion of sandy loam and silty loam and silt reaching 72.5%. The lowest TSS appears in sandy soil and loamy sand, at 13,140 mg/kg, while the highest value appears in silty loam and silt, at 68,930 mg/kg, with the overall TSS of sandy soil and loamy sand being lower than that of the other soil types.

**Table 7.** Statistical analysis of soil salinity and soil particle size under different soil texture types.

| Soil Texture Type | Layers (cm) | Samples | Clay (%) | Silt (%) | Sand (%) | $D_{soil}$ | Average Salt Content (mg/kg) |
|---|---|---|---|---|---|---|---|
| Sandy soil; loamy sandy soil | 0–10 | 14 | 3.61 | 26.01 | 70.39 | 2.49 | 35,730 |
| | 10–20 | 11 | 2.19 | 16.78 | 81.03 | 2.40 | 14,950 |
| | 20–40 | 17 | 1.80 | 15.27 | 82.93 | 2.36 | 13,140 |
| | 40–60 | 13 | 1.76 | 14.37 | 83.88 | 2.36 | 15,200 |
| Sandy loam; loam | 0–10 | 28 | 6.22 | 50.85 | 42.93 | 2.59 | 43,490 |
| | 10–20 | 19 | 4.49 | 32.24 | 63.28 | 2.53 | 26,770 |
| | 20–40 | 14 | 5.52 | 36.34 | 58.14 | 2.57 | 19,780 |
| | 40–60 | 17 | 4.88 | 36.27 | 58.85 | 2.55 | 16,630 |
| Silt; silty loam | 0–10 | 8 | 7.17 | 60.58 | 32.24 | 2.62 | 68,930 |
| | 10–20 | 20 | 7.07 | 57.25 | 35.68 | 2.61 | 27,640 |
| | 20–40 | 19 | 7.58 | 63.53 | 28.88 | 2.62 | 24,311 |
| | 40–60 | 20 | 7.78 | 60.98 | 31.25 | 2.62 | 23,071 |

Figure 9 shows the differences in the contents of TSS and salt ions in different soil textures. $CO_3^{2-}$ was excluded from the analytical section below due to the lack of $CO_3^{2-}$ in most of the samples, resulting in low $CO_3^{2-}$ levels and large errors. Overall, TSS and salt ions were highest in the 0–10 cm, with most ions showing a decrease in content with increasing soil depth. TSS, $Cl^-$, $SO_4^{2-}$, $Ca^{2+}$, $Mg^{2+}$, $Na^+ + K^+$ content increased with finer soil texture in different soil textures, except for $HCO_3^-$ ions. In 0–20 cm, TSS, $Cl^-$, $Mg^{2+}$, and $Na^+ + K^+$ were more variable, with reductions ranging from 53 to 75%, and in 20–60 cm, the variations leveled off, with variations ranging from 0.5 to 14.5%. From 0 to 60 cm, the reduction of $HCO_3^-$, $SO_4^{2-}$, and $Ca^{2+}$ varied between 0.1 and 36%, with small variations. $HCO_3^-$ and $SO_4^{2-}$ content varied little in different soil textures, with an overall "S" pattern. In summary, the average TSS content of the soil gradually increased as the soil texture became finer and $D_{soil}$ increased. It also showed that there were significant differences in the migration of different salt ions across the soil profile.

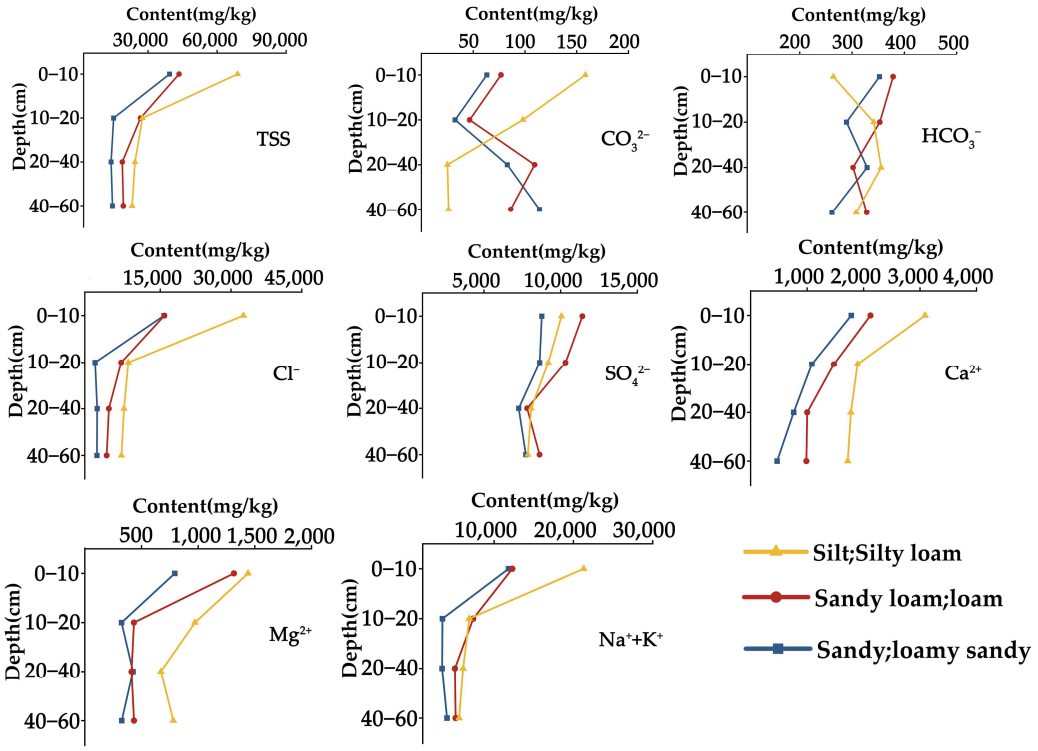


**Figure 9.** TSS and salt ion contents in different soil textures.

## 4. Discussion

### *4.1. Analysis of Distribution Characteristics of Salinity and Salt Ions*

The accumulation of surface soil salinity in the study area was prominent, and there was an interrelationship between the salinity levels at different soil depths. This was consistent with the findings in the Pariette Draw wetland in the United States, where capillary water movement caused soil salinity accumulation in the surface layer of wetland soils [66]. In the Ebinur Lake wetlands, soil salinity is strongly influenced by regional climate and topography. Redundancy analysis results clearly indicated that topographic and climatic factors had a significant impact on salt accumulation (Figure S3, Table S2). And freshwater wetlands located in dryland environments are characterized by high evapotranspiration rates and frequent periods of desiccation [67]. High temperatures and strong evapotranspiration during seasonal peaks cause shallow groundwater to migrate continuously to the surface, carrying salt-rich water that evaporates at the surface [68]. With a reduction in water content, the evaporation rate gradually declines, and the temperature decreases with increasing soil depth. The evaporation front is unable to move downward due to groundwater replenishment, and deeper soils are less influenced by evaporation [69]. Analyzing the $Cl^-/SO_4{}^{2-}$ equivalent ratios revealed asynchronous migration rates of different salt ions in the soil profile, with $Cl^-$, which was highly mobile during upward migration, moving quickly through the soil, while $SO_4{}^{2-}$, having low solubility, migrated relatively slowly. Additionally, the correlation between $Cl^-$ and $Na^+ + K^+$ was the strongest in the soil profile, indicating synergistic transport of these ions, likely due to differences in their solubility, mobility, and microtopographic distribution [70]. Zhang et al. also showed that the water–salt migration changes in Ebinur Lake were influenced by microgeomorphology, soil texture, and other factors [71]. Therefore, during the upward mobilization of labile salts in the study area, chloride upward epimerization was the strongest, followed by sulfate. Additionally, human activities have played an indirect role in promoting the accumulation of soil salinity [72]. Ainur indicated that salt content increased significantly from west to east in the Bortala River Basin, with the most severe salinization occurring in the Ebinur Lake wetland at the eastern end of the basin, suggesting irrigation's impact on salt accumulation and migration [73]. Excessive agricultural irrigation has reduced downstream surface runoff, even causing streamflow cessation, leading to the shrinkage of the Ebinur Lake area [47]. Under intense wind erosion in Alashankou, the exposed dried lakebed becomes one of the primary sources of saline dust storms [40]. This secondary landscape results from hydrological imbalances, reduced saline lake areas, the evaporation of saline lake waters, and salt accumulation on dried lakebeds [74]. Similar issues of saline dust storms were observed in the Aral Sea, driven by declining water levels and drought [75].

### *4.2. Fractal Dimension of Particle Size Distribution*

Fractal dimension is an important parameter commonly used to characterize PSD [76]. Previous studies have shown that finer-textured, nutrient-rich soils generally have fractal dimensions of 2.60 to 2.80, and coarser-grained, less structured soils have fractal dimensions of 1.83 to 2.6453 [77]. Furthermore, Liu et al. indicated that well-structured soils tend to have a fractal dimension of approximately 2.75 [78]. In this study, the fractal dimension ranges from 1.91 to 2.76, with an average value of 2.54. Most of the $D_{soil}$ values in this study were less than 2.75, indicating poor soil structure and a high sand content in the study area. According to Table 7, the combined proportion of sandy loam, silty loam, and silt in the soil profile reached 72.5%, indicating dominance by sandy and loamy soils with coarse texture and poor structure, which are unfavorable for retaining soil moisture and nutrients, resulting in relatively low soil fertility. In the soil profile, $D_{soil}$ showed highly significant correlations with both soil particle size (Figure S2), highly significant negative correlations

with sand ($p < 0.01$), and significant positive correlations with silt and clay ($p < 0.01$), with correlations above 0.8. The results confirmed that the finer the particle size, the greater the soil fractal dimension. These correlations indicated the usefulness of fractal dimension to characterize the PSD of saline soils.

### *4.3. Analysis of Relationship Between Soil Salinity and Soil Particle Size*

Numerous studies to date have demonstrated a significant relationship between soil particle size and soil moisture, nutrients, and soil organic matter [39,79]. Soil texture and its vertical spatial heterogeneity may greatly influence the distribution of water and solutes in the soil profile [38], which is one of the important factors affecting salt ion retention [80]. The results of this study showed that TSS was positively correlated with $D_{soil}$, clay, and silt and negatively correlated with sand. At the same time, there were differences in salinity among different soil textures, mainly in the form of an increasing trend in TSS and $D_{soil}$ with the increase in the fine-grained fraction. This may be due to the strong evaporation from the surface in summer [81], and the fact that soil texture in the vertical profile is dominated by sandy loam, loam, silty loam, and silt, and that sandy loam to silty loam have moderate sized capillary porosity compared to sandy loam and clay, and that groundwater rises through the soil capillaries at a faster rate and at a higher altitude [82], making the soils more susceptible to salinization. Meantime, areas with a higher distribution of sand exhibit higher permeability due to larger particles and porosity, resulting in a weaker salt-holding and adsorption capacity as salts are more likely to migrate deeper with water [83]. There were differences in the strength of correlations between $D_{soil}$ and the various salt ions at different soil depths, with $D_{soil}$ being significantly positively correlated with $Cl^-$ and $Na^+ + K^+$ in the soil profile, and cations generally having higher correlations with $D_{soil}$ than anions. Furthermore, Chen et al. modified the soil particle size composition and texture by varying the content of shell sand, revealing that the leaching rate of salt ions differed with varying shell sand contents [84]. This indicated that the PSD of the soil profile might be a driving factor affecting the migration of different soluble cations and anions [85], resulting in an increased $Cl^-/SO_4^{2-}$ equivalent ratio from the bottom to the top of the vertical profile. Due to the seasonal nature of wetlands, NaCl was eventually lost through surface evaporation and accumulated on the soil surface. The impact of excessive soil salinity on wetland ecosystems is destructive and long-lasting. The relationship between soil salinity and soil particle size presented in the study area provides a basis for understanding the effect of soil particle size on soil salinity and acts as a reference point for wetlands with similar environments. In addition to the results of this study, Wang et al. indicated that controlling the lake area of Ebinur Lake had a positive effect on the ecological restoration of the wetland [47].

## 5. Conclusions

In this study, soil profile samples of 0–60 cm from Ebinur Lake wetland were analyzed by combining Pearson correlation, IDW spatial interpolation, and redundancy analysis to explore the relationship between soil particle size and soil salinity, and to reveal the characteristics of vertical distribution of soil salinity and its influencing factors. The results indicated that the Ebinur Lake wetland was severely salinized, with pronounced surface soil salinity accumulation. The dominant salinization type was chloride, with $Cl^-$ and $Na^+ + K^+$ playing major roles in the salinization process. TSS were significantly and positively correlated with Dsoil. Salt content varied among soil textures, with more pronounced salt accumulation in finer soil particles, particularly in sandy loam and silt soils. This study demonstrated that PSD is closely related to soil salinity, while climate, topography, and geomorphology also significantly influenced soil salt accumulation in the Ebinur

Lake wetland. The findings are expected to provide valuable insights into wetland soil management and ecological restoration.

**Supplementary Materials:** The following supporting information can be downloaded at: https://www.mdpi.com/article/10.3390/land14020297/s1. Figure S1: Three-phase plot of soil particle size distribution in the soil surface layer (0–10); Figure S2: Soil fractal dimensions in relation to clay, silt, sand, and TSS; Figure S3: The relationship between total salt content at different depths and related factors. Notes: TSS1, TSS2, TSS3, and TSS4 represent soil salinity at depths of 0–10, 10–20, 20–40, and 40–60 cm, respectively; DEM represents digital elevation model; Aspect refers to slope aspect; Slope indicates slope steepness; PRE refers to precipitation in August 2023; TEM denotes the average temperature in August 2023; LUCC represents land use/land cover in 2023; Table S1: Soil texture types at different soil depths; Table S2: A ranking of environmental factors based on Monte Carlo testing.

**Author Contributions:** D.W.: Conceptualization, Methodology, Software, Data Curation, Visualization, Writing—Original Draft, Writing—Review and Editing. J.W.: Resources, Funding Acquisition Supervision, Writing—Review and Editing, Project Administration. J.D.: Supervision, Writing—Review and Editing, Project Administration. Z.Z.: Data Curation, Conceptualization, Supervision. All authors have read and agreed to the published version of the manuscript.

**Funding:** This research was funded by the Innovation Team for Efficient Utilization of Water Resources in Arid Zones (2022TSYCTD0001); the Basic Resources Investigation Project of the Ministry of Science and Technology: Water Resources Investigation and carrying capacity assessment of Turpan–Hami Basin (2021xjkk1000); and the University Scientific Research Plan of the Education Department of Xinjian Uygur Autonomous Region (XJEDU2021Y009).

**Data Availability Statement:** Data will be made available on request.

**Conflicts of Interest:** The authors declare no conflicts of interest.

## References

1. Herbert, E.R.; Boon, P.; Burgin, A.J.; Neubauer, S.C.; Franklin, R.B.; Ardón, M.; Hopfensperger, K.N.; Lamers, L.P.; Gell, P. A global perspective on wetland salinization: Ecological consequences of a growing threat to freshwater wetlands. *Ecosphere* **2015**, *6*, 1–43. [CrossRef]
2. Suleymanov, A.; Gabbasova, I.; Komissarov, M.; Suleymanov, R.; Garipov, T.; Tuktarova, I.; Belan, L. Random forest modeling of soil properties in saline semi-arid areas. *Agriculture* **2023**, *13*, 976. [CrossRef]
3. Andrade Foronda, D.; Colinet, G. Prediction of soil salinity/sodicity and salt-affected soil classes from soluble salt ions using machine learning algorithms. *Soil Syst.* **2023**, *7*, 47. [CrossRef]
4. Singh, A. Soil salinity: A global threat to sustainable development. *Soil Use Manag.* **2022**, *38*, 39–67. [CrossRef]
5. Zhuang, Q.; Shao, Z.; Huang, X.; Zhang, Y.; Wu, W.; Feng, X.; Lv, X.; Ding, Q.; Cai, B.; Altan, O. Evolution of soil salinization under the background of landscape patterns in the irrigated northern slopes of Tianshan Mountains, Xinjiang, China. *Catena* **2021**, *206*, 105561. [CrossRef]
6. Wang, J.; Wu, J.; Jia, H. Analysis of spatial variation of soil salinization using a hydrochemical and stable isotopic method in a semiarid irrigated basin, Hetao Plain, inner Mongolia, North China. *Environ. Process.* **2016**, *3*, 723–733. [CrossRef]
7. Chernousenko, G.; Oreshnikova, N.; Ukraintseva, N. Soil salinization in coastal areas of the Arctic and Pacific regions of Russia. *Eurasian Soil Sci. C/C Pochvovedenie* **2001**, *34*, 1062–1076.
8. Herrero, J.; Pérez-Coveta, O. Soil salinity changes over 24 years in a Mediterranean irrigated district. *Geoderma* **2005**, *125*, 287–308. [CrossRef]
9. Gebremeskel, G.; Gebremicael, T.; Kifle, M.; Meresa, E.; Gebremedhin, T.; Girmay, A. Salinization pattern and its spatial distribution in the irrigated agriculture of Northern Ethiopia: An integrated approach of quantitative and spatial analysis. *Agric. Water Manag.* **2018**, *206*, 147–157. [CrossRef]
10. Zheng, M.; Bai, Y.; Zhang, J.; Ding, B.; Xiao, J. Soil salinity characteristics of typical oasis in arid area based on principal component analysis: An example in Xinjiang. *Chin. Agric. Sci. Bull.* **2020**, *36*, 81–87.
11. Li, Q.; Xi, M.; Wang, Q.; Kong, F.; Li, Y. Characterization of soil salinization in typical estuarine area of the Jiaozhou Bay, China. *Phys. Chem. Earth Parts A/B/C* **2018**, *103*, 51–61. [CrossRef]

12. Burgess, T.; Webster, R. Optimal interpolation and isarithmic mapping of soil properties: I The semi-variogram and punctual kriging. *J. Soil Sci.* **1980**, *31*, 315–331. [CrossRef]
13. Liu, G.; Li, J.; Zhang, X.; Wang, X.; Lv, Z.; Yang, J.; Shao, H.; Yu, S. GIS-mapping spatial distribution of soil salinity for Eco-restoring the Yellow River Delta in combination with electromagnetic induction. *Ecol. Eng.* **2016**, *94*, 306–314. [CrossRef]
14. Yang, Z.; Wang, B. Present status of saline soil resources and countermeasures for improvement and utilization in China. *Shandong Agric. Sci.* **2015**, *47*, 125–130.
15. Singh, A. Soil salinization management for sustainable development: A review. *J. Environ. Manag.* **2021**, *277*, 111383. [CrossRef]
16. Zhang, Y.; Hou, K.; Qian, H.; Gao, Y.; Fang, Y.; Tang, S.; Xiao, S.; Ren, W.; Qu, W.; Zhang, Q. Natural-human driving factors of groundwater salinization in a long-term irrigation area. *Environ. Res.* **2023**, *220*, 115178. [CrossRef]
17. Zhang, J.; Cai, J.; Xu, D.; Wu, B.; Chang, H.; Zhang, B.; Wei, Z. Soil salinization poses greater effects than soil moisture on field crop growth and yield in arid farming areas with intense irrigation. *J. Clean. Prod.* **2024**, *451*, 142007. [CrossRef]
18. Akramkhanov, A.; Martius, C.; Park, S.J.; Hendrickx, J.M. Environmental factors of spatial distribution of soil salinity on flat irrigated terrain. *Geoderma* **2011**, *163*, 55–62. [CrossRef]
19. Sharma, L.K.; Naik, R. Saline Wetland Ecosystems. In *Conservation of Saline Wetland Ecosystems: An Initiative towards UN Decade of Ecological Restoration*; Springer: Singapore, 2024; pp. 33–75.
20. Nurbekova, Z.; Satkanov, M.; Beisekova, M.; Akbassova, A.; Ualiyeva, R.; Cui, J.; Chen, Y.; Wang, Z.; Zhangazin, S. Strategies for achieving high and sustainable plant productivity in saline soil conditions. *Horticulturae* **2024**, *10*, 878. [CrossRef]
21. Liu, Y. The driving factors and ecological countermeasures of soil salinization in the seawater intrusion areas in the south of Laizhou Bay. *Chin. Agric. Sci. Bull.* **2012**, *19*, 193–204.
22. Li, E.; Shen, J.; Jing, J.; Hu, H.; Lu, X. Distribution characteristics of salinity and nutrient at the estuary in coastal saline soil of north Jiangsu. *Sci. Soil Water Conserv.* **2016**, *14*, 79–88.
23. Cañedo-Argüelles, M.; Kefford, B.J.; Piscart, C.; Prat, N.; Schäfer, R.B.; Schulz, C.-J. Salinisation of rivers: An urgent ecological issue. *Environ. Pollut.* **2013**, *173*, 157–167. [CrossRef] [PubMed]
24. Cao, S.-Y.; Guo, Q.-E.; Che, Z.-X.; Gao, Y.; Ge, H.-J. Effects of phosphate gypsum agent on soil moisture diffusivity. *Arid Zone Res.* **2016**, *33*, 506–510.
25. Stavi, I.; Thevs, N.; Priori, S. Soil salinity and sodicity in drylands: A review of causes, effects, monitoring, and restoration measures. *Front. Environ. Sci.* **2021**, *9*, 712831. [CrossRef]
26. Fu, X.; Wu, X.; Wang, H.; Chen, Y.; Wang, R.; Wang, Y. Effects of fertigation with carboxymethyl cellulose potassium on water conservation, salt suppression, and maize growth in salt-affected soil. *Agric. Water Manag.* **2023**, *287*, 108436. [CrossRef]
27. Xie, X.; Pu, L.; Zhu, M.; Xu, Y.; Wang, X. Linkage between soil salinization indicators and physicochemical properties in a long-term intensive agricultural coastal reclamation area, Eastern China. *J. Soils Sediments* **2019**, *19*, 3699–3707. [CrossRef]
28. Hu, H.; Tian, F.; Hu, H. Soil particle size distribution and its relationship with soil water and salt under mulched drip irrigation in Xinjiang of China. *Sci. China Technol. Sci.* **2011**, *54*, 1568–1574. [CrossRef]
29. Rubinić, V.; Lazarević, B.; Husnjak, S.; Durn, G. Climate and relief influence on particle size distribution and chemical properties of pseudogley soils in croatia. *Catena* **2015**, *127*, 340–348. [CrossRef]
30. Zhang, Y.; Hou, K.; Qian, H.; Gao, Y.; Fang, Y.; Xiao, S.; Tang, S.; Zhang, Q.; Qu, W.; Ren, W. Characterization of soil salinization and its driving factors in a typical irrigation area of Northwest China. *Sci. Total Environ.* **2022**, *837*, 155808. [CrossRef]
31. Shokri, N.; Hassani, A.; Sahimi, M. Multi-scale soil salinization dynamics from global to pore scale: A review. *Rev. Geophys.* **2024**, *62*, e2023RG000804. [CrossRef]
32. Gao, Z.; Niu, F.; Lin, Z.; Luo, J. Fractal and multifractal analysis of soil particle-size distribution and correlation with soil hydrological properties in active layer of Qinghai–Tibet Plateau, China. *Catena* **2021**, *203*, 105373. [CrossRef]
33. Richer-de-Forges, A.C.; Arrouays, D.; Chen, S.; Dobarco, M.R.; Libohova, Z.; Roudier, P.; Minasny, B.; Bourennane, H. Hand-feel soil texture and particle-size distribution in central France. Relationships and implications. *Catena* **2022**, *213*, 106155. [CrossRef]
34. Song, X.Y.; Li, H.Y. Fractal characteristics of soil particle-size distributions under different landform and land-use types. *Adv. Mater. Res.* **2011**, *201*, 2679–2684. [CrossRef]
35. Zhang, A.; Ding, J.; Wang, J.; SaiDi, M.; Li, Y. Fractal and multifractal analysis on saline soil particle size distribution in arid oasis. *Arid Zone Res.* **2019**, *36*, 314–322.
36. Wang, E.; Chen, J.; Liu, L.; Cui, L.; Xue, J.; Ren, J.; Du, Q. Effect of soil texture on water and salt transport in freeze—Thaw soil in the shallow groundwater area. *Water* **2023**, *15*, 2587. [CrossRef]
37. Bing, H.; He, P.; Zhang, Y. Cyclic freeze–thaw as a mechanism for water and salt migration in soil. *Environ. Earth Sci.* **2015**, *74*, 675–681. [CrossRef]
38. Li, X.; Chang, S.X.; Salifu, K.F. Soil texture and layering effects on water and salt dynamics in the presence of a water table: A review. *Environ. Rev.* **2014**, *22*, 41–50. [CrossRef]
39. Zettl, J.; Lee Barbour, S.; Huang, M.; Si, B.; Leskiw, L. Influence of textural layering on field capacity of coarse soils. *Can. J. Soil Sci.* **2011**, *91*, 133–147. [CrossRef]

40. Liu, Y.; Wang, X.; Wu, Y. Research on the water level change effect on the salinity of everglade around Ebinur Lake. *J. Arid Land Resour. Environ.* **2010**, *24*, 108–111.
41. Ding, J.-L.; Ge, X.-Y.; Wang, J.-Z. Ebinur Lake wetland identification and its spatio-temporal dynamic changes. *J. Nat. Resour.* **2021**, *36*, 1949–1963. [CrossRef]
42. Xie, W.; Wu, L.; Zhang, Y.; Wu, T.; Li, X.; Ouyang, Z. Effects of straw application on coastal saline topsoil salinity and wheat yield trend. *Soil Tillage Res.* **2017**, *169*, 1–6. [CrossRef]
43. Xue, L.; Jiang, J.; Li, X.; Yan, Z.; Zhang, Q.; Ge, Z.; Tian, B.; Craft, C. Salinity affects topsoil organic carbon concentrations through regulating vegetation structure and productivity. *J. Geophys. Res. Biogeosci.* **2020**, *125*, e2019JG005217. [CrossRef]
44. Nguyen, V.H.; Germer, J.; Asch, F. Evaluating topsoil salinity via geophysical methods in rice production systems in the Vietnam Mekong Delta. *J. Agron. Crop Sci.* **2024**, *210*, e12676. [CrossRef]
45. Guo, Q.-E.; Cao, S.-Y.; Zhan, Z.-B.; Nan, L.-L.; Wang, Z.; Zhang, J.-J.; Zhu, X.-T. Distribution characteristics of salt ions in soil particles of different grain sizes of two typical salt-forming soils in Gansu. *Arid Zone Agric. Res.* **2021**, *5*, 216–221.
46. He, B.; Hu, W.; Chen, X.; Ding, C.; Qi, X. Spatial and temporal distribution characteristics and diversity of myxobacteria in the rhizosphere of Phragmites australis in Ebinur Lake wetland. *Acta Microbiol. Sin.* **2024**, *4*.
47. Wang, J.; Ding, J.; Yu, D.; Ma, X.; Zhang, Z.; Ge, X.; Teng, D.; Li, X.; Liang, J.; Lizaga, I. Capability of Sentinel-2 MSI data for monitoring and mapping of soil salinity in dry and wet seasons in the Ebinur Lake region, Xinjiang, China. *Geoderma* **2019**, *353*, 172–187. [CrossRef]
48. Yuan, Y.; Fu, D.; Lü, G. Inter-specific relations of the dominant plants of the wetland vegetation in the Ebinur Lake Wetland in Xinjiang Uygur autonomous region. *Wetl. Sci.* **2008**, *6*, 486–491.
49. Abulimiti, A.; Wang, Y.-H. Soil organic matter, salinity, and water content in the Aibi Lake Wetland. *J. Northeast. For. Univ.* **2020**, *48*, 34–40.
50. Sun, Q.; Sun, J.; Baidurela, A.; Li, L.; Hu, X.; Song, T. Ecological landscape pattern changes and security from 1990 to 2021 in Ebinur Lake Wetland Reserve, China. *Ecol. Indic.* **2022**, *145*, 109648. [CrossRef]
51. Gondek, M.; Weindorf, D.C.; Thiel, C.; Kleinheinz, G. Soluble salts in compost and their effects on soil and plants: A review. *Compos. Sci. Util.* **2020**, *28*, 59–75. [CrossRef]
52. Richards, L. Diagnosis and improvement of saline. *Saline Alkali Soils. Handb.* **1954**, *60*, 129–134.
53. Hardie, M.; Doyle, R. Measuring soil salinity. In *Plant Salt Tolerance. Methods in Molecular Biology*; Humana Press: Totowa, NJ, USA, 2012; pp. 415–425.
54. Choudhary, O.; Kharche, V.K. Soil salinity and sodicity. *Soil Sci.* **2018**, *12*, 353–384.
55. Rhoades, J. Salinity: Electrical conductivity and total dissolved solids. *Methods Soil Anal.* **1996**, *5 Pt 3*, 417–435.
56. Zhao, Y.; Feng, Q.; Yang, H. Soil salinity distribution and its relationship with soil particle size in the lower reaches of Heihe River, Northwestern China. *Environ. Earth Sci.* **2016**, *75*, 810. [CrossRef]
57. Wang, G.L.; Zhou, S.L.; Zhao, Q.G. Volume fractal dimension of soil particles and its applications to land use. *Acta Pedol. Sin.* **2005**, *42*, 546–550.
58. Zhao, W.; Cao, T.; Li, Z.; Sheng, J. Comparison of IDW, cokriging and ARMA for predicting spatiotemporal variability of soil salinity in a gravel–sand mulched jujube orchard. *Environ. Monit. Assess.* **2019**, *191*, 376. [CrossRef]
59. Liu, Q.; Zhang, H.-W.; Shi, Y.-X. The pollution assessment and spatial distribution of soil heavy metals in field scale—Case study in Yanggu county of northwest Shandong province. *Chin. J. Soil Sci.* **2009**, *40*, 673–678.
60. Zhang, X.; Zhao, W.; Wang, L.; Liu, Y.; Liu, Y.; Feng, Q. Relationship between soil water content and soil particle size on typical slopes of the Loess Plateau during a drought year. *Sci. Total Environ.* **2019**, *648*, 943–954. [CrossRef]
61. Zhang, T.; Zhan, X.; He, J.; Feng, H.; Kang, Y. Salt characteristics and soluble cations redistribution in an impermeable calcareous saline-sodic soil reclaimed with an improved drip irrigation. *Agric. Water Manag.* **2018**, *197*, 91–99. [CrossRef]
62. Juan, P.; Mateu, J.; Jordan, M.; Mataix-Solera, J.; Meléndez-Pastor, I.; Navarro-Pedreño, J. Geostatistical methods to identify and map spatial variations of soil salinity. *J. Geochem. Explor.* **2011**, *108*, 62–72. [CrossRef]
63. Fu, T.; Gao, H.; Liu, J. Comparison of different interpolation methods for prediction of soil salinity in arid irrigation region in northern China. *Agronomy* **2021**, *11*, 1535. [CrossRef]
64. Wang, J.; Ding, J.; Wang, F.; Liang, J. Study on particle size composition and erodibility of different salinized soils in Ebinur Lake wetland. *Soil* **2018**, *50*, 598–605.
65. Caputo, M.C.; De Carlo, L.; Turturro, A.C. HYPROP-FIT to model rock water retention curves estimated by different methods. *Water* **2022**, *14*, 3443. [CrossRef]
66. Jones, C.P.; Grossl, P.R.; Amacher, M.C.; Boettinger, J.L.; Jacobson, A.R.; Lawley, J.R. Selenium and salt mobilization in wetland and arid upland soils of Pariette Draw, Utah (USA). *Geoderma* **2017**, *305*, 363–373. [CrossRef]
67. Humphries, M.; McCarthy, T. Chemical sedimentation as a driver of habitat diversity in dryland wetlands. *Wetl. Ecol. Manag.* **2022**, *30*, 675–694. [CrossRef]

68. Jia, Y.; Guo, H.; Xi, B.; Jiang, Y.; Zhang, Z.; Yuan, R.; Yi, W.; Xue, X. Sources of groundwater salinity and potential impact on arsenic mobility in the western Hetao Basin, Inner Mongolia. *Sci. Total Environ.* **2017**, *601*, 691–702. [CrossRef]
69. Zhao, X.; He, X.; Yang, X.; Zhang, X.; Lv, G. Effects of soil moisture and salt on desert plant biodiversity in Ebinur Lake Basin of Xinjiang. *China. J. Arid Land Resour. Environ.* **2017**, *31*, 76–82.
70. Vepraskas, M.J.; Craft, C.B. *Wetland Soils: Genesis, Hydrology, Landscapes, and Classification*; CRC Press: Boca Raton, FL, USA, 2016.
71. Zhang, X.; Li, Y.; Li, F. Spatial distribution characteristics of soil water-salt gradients in the ecological buffer zone of arid zone lakes and their influencing factors. *J. Clean. Prod.* **2024**, *444*, 141299. [CrossRef]
72. Xie, W.; Yang, J.; Yao, R.; Wang, X. Impact study of impoundment of the three gorges reservoir on salt-water dynamics and soil salinity in the Yangtze River estuary. *J. Environ. Inform.* **2020**, *36*, 11–23. [CrossRef]
73. Tiliwalidi, A. Study on Spatial Variability of Soil Salinity and Its Influencing Factors in the Bortala River Basin. Master's Thesis, Xinjiang University, Urumqi, China, 2013.
74. Wurtsbaugh, W.A.; Miller, C.; Null, S.E.; DeRose, R.J.; Wilcock, P.; Hahnenberger, M.; Howe, F.; Moore, J. Decline of the world's saline lakes. *Nat. Geosci.* **2017**, *10*, 816–821. [CrossRef]
75. Opp, C.; Groll, M.; Abbasi, H.; Foroushani, M.A. Causes and effects of sand and dust storms: What has past research taught us? A survey. *J. Risk Financial Manag.* **2021**, *14*, 326. [CrossRef]
76. Tyler, S.W.; Wheatcraft, S.W. Fractal scaling of soil particle-size distributions: Analysis and limitations. *Soil Sci. Soc. Am. J.* **1992**, *56*, 362–369. [CrossRef]
77. Bai, Y.; Qin, Y.; Lu, X.; Zhang, J.; Chen, G.; Li, X. Fractal dimension of particle-size distribution and their relationships with alkalinity properties of soils in the western Songnen Plain, China. *Sci. Rep.* **2020**, *10*, 20603. [CrossRef] [PubMed]
78. Liu, X.; Zhang, G.; Heathman, G.C.; Wang, Y.; Huang, C.-h. Fractal features of soil particle-size distribution as affected by plant communities in the forested region of Mountain Yimeng, China. *Geoderma* **2009**, *154*, 123–130. [CrossRef]
79. Martín, M.Á.; Montero, E.S. Laser diffraction and multifractal analysis for the characterization of dry soil volume-size distributions. *Soil Tillage Res.* **2002**, *64*, 113–123. [CrossRef]
80. Gui, D.; Lei, J.; Zeng, F.; Mu, G.; Zhu, J.; Wang, H.; Zhang, Q. Characterizing variations in soil particle size distribution in oasis farmlands—A case study of the Cele Oasis. *Math. Comput. Model.* **2010**, *51*, 1306–1311. [CrossRef]
81. Amantai, N.; Ding, J.; Ge, X.; Bao, Q. Variation characteristics of actual evapotranspiration and meteorological elements in the Ebinur Lake basin from 1960 to 2017. *Acta Geogr. Sin* **2021**, *76*, 1177–1192.
82. Smith, W. Infiltration in sands and its relation to groundwater recharge. *Water Resour. Res.* **1967**, *3*, 539–555. [CrossRef]
83. Wang, P.; Hu, F.; Han, Z.; Kong, X. Experimental study on dispersion of saline water flowing through clay-bearing soil. South North Water Transf. *Water Sci. Technol.* **2014**, *12*, 101–104.
84. Chen, P.; Sun, J.; Ma, L.; Chen, Y.; Xia, J. Effects of shell sand content on soil physical properties and salt ions under simulated rainfall leaching. *Geoderma* **2022**, *406*, 115520. [CrossRef]
85. Wang, J.; Liu, Y.; Wang, S.; Liu, H.; Fu, G.; Xiong, Y. Spatial distribution of soil salinity and potential implications for soil management in the Manas River watershed, China. *Soil Use Manag.* **2020**, *36*, 93–103. [CrossRef]